Steel and Composite Structures, *Vol. 31*, *No. 3* (*2019*) *303-317*
DOI: https://doi.org/10.12989/scs.2019.31.3.303

Behaviour and design of high-strength steel beam-to-column joints

Dongxu Li*, Brian Uy [a] and Jia Wang [b]

School of Civil Engineering, *The University of Sydney*, *Sydney*, *NSW 2006*, *Australia*

(*Received December 16*, *2018*, *Revised April 5*, *2019*, *Accepted April 11*, *2019*)

Abstract. This paper presents a finite element model for predicting the behaviour of high-strength steel bolted beam-to-column joints under monotonic loading. The developed numerical model considers the effects of material nonlinearities and geometric nonlinearities. The accuracy of the developed model is examined by comparing the predicted results with independent experimental results. It is demonstrated that the proposed model accurately predicts the ultimate flexural resistances and moment-rotation curves for high-strength steel bolted beam-to-column joints. Mechanical performance of three joint configurations with various design details is examined. A parametric study is carried out to investigate the effects of key design parameters on the behaviour of bolted beam-to-column joints with double-extended endplates. The plastic flexural capacities of the beam-to-column joints from the experimental programme and numerical analysis are compared with the current codes of practice. It is found that the initial stiffness and plastic flexural resistance of the high-strength steel beam-to-column joints are overestimated. Proper modifications need to be conducted to ensure the current analytical method can be safely used for the bolted beam-to-column joints with high-performance materials.

Keywords: high-strength steel; beam-to-column joint; numerical analysis; design codes

1. Introduction

High-strength steel (HSS) is a relatively new generation of structural steel that has exhibited enhanced mechanical properties over conventional mild steel. Based on the current manufacturing technology, HSS is normally produced through the thermo-mechanical process or quenched and tempered process. HSS represents a family of structural steels with a nominal yield strength over 460 MPa and offers higher performance in tensile stress, toughness, weldability and corrosion resistance compared to the conventional mild steel grades (Günther 2005). The most significant advantage of using HSS is the reduced weight of the structural members. With the higher strength being utilised, the dimensions of the structural members can be reduced considerably, which lead to further cost savings, such as less welding, transportation and erection costs (Gogou 2012).

Despite all these advantages of HSS, several concerns from the construction industry still limit the wider application of this type of structural steel. One of these limitations is that the initial costs for HSS are higher than conventional mild steels (Shi *et al*. 2012, Li *et al*. 2016c). Moreover, the current international design provisions just allow the HSS with a nominal yield strength up to 690 MPa to be utilised, such as AS4100 (1998), AS/NZS 5100.6 (2017), AS/NZS 2327 (2017) and EC3-1-12 (Eurocode 2007). However, most of the design requirements for steel members and joints are still based on the conventional mild steels. The concerns about the ductility of HSS members and lack of sufficient plastic deformation of joints with these high-performance materials significantly limits their application. These concerns have also influenced the design concepts that are used in the current codes of practice, which only allow the elastic behaviour of HSS to be used for design purposes (Coelho *et al*. 2006). Thus, there exists an increasing awareness that more research on joints with HSS should be performed. The applicability of plastic analysis on high performance steel members and joints should be investigated to avoid over design, through which the benefits of HSS can be fully utilised.

In a typical steel frame structure, the behaviour of beam-to-column joint is more complex than the connected steel members owing to the discontinuities in the connection zones (Fig. 1). Many design details could potentially affect the performance of these types of joint, such as the bolt strength and diameter, endplate type and thickness, as well as the presence of stiffeners in the connected members. The complexity of this joint behaviour and the significant influences on the global analysis of steel frames has been attracting the attention from researchers. Abidelah et al. (2012), Augusto *et al*. (2016), Morrison *et al*. (2017), Tartaglia *et al*. (2018) and Francavilla *et al*. (2018) performed both experimental and numerical analysis on bolted steel beam-to-column joints with open section members, the effects of various design parameters were investigated. More recently, Liu *et al*. (2017) and Tahir *et al*. (2018) proposed innovative joints to connect steel beams and box columns, the prefabricated members can be readily assembled through the bolted connections.

In addition to the bolted steel beam-to-column joints,

*Corresponding author, Ph.D., Research Associate,
E-mail: dongxu.li@sydney.edu.au
[a] Ph.D., Professor
[b] Ph.D., Research Associate

http://www.techno-press.org/?journal=scs&subpage=6
ISSN: 1229-9367 (Print), 1598-6233 (Online)

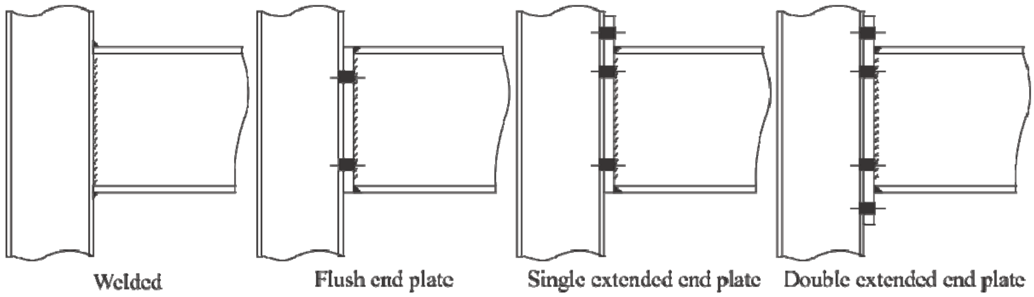

Fig. 1 Commonly used steel beam-to-column joints

Kim and Oh (2007), Goswami and Murty (2010), Mirghaderi *et al*. (2010), Gholami *et al*. (2013) and Ge *et al*. (2014) examined the mechanical performance of welded steel beam-to-column joints. In these researches, the focus was to involve different stiffeners in the endplates and column webs. The effects of these additional stiffeners on the moment resisting capacity of the joints under cyclic loading were investigated. However, a welded connection cannot be easily disassembled after its useful service life. Instead, the bolted joints between the connected beams and columns could facilitate the dismantling of steel members after their service life (Uy *et al*. 2017). This could encourage the concept of sustainability and reuse of steel components in the construction industry to be achieved. Furthermore, it is worth noting that the above-mentioned research utilised mild structural steel for connected beams, columns and endplates.

Over the past few years, there has been increasing interest in using HSS for structural members. Ban *et al*. (2013) investigated the buckling behaviour of ultra-high strength steel members under axial compression. Uy (2001) and Chen *et al*. (2006) firstly investigated the mechanical performance of HSS and utilised this type of material in concrete-filled steel tubular composite columns. Portoles *et al*. (2013), Thai *et al*. (2014), Skalomenos *et al*. (2016), Du *et al*. (2017) and Xiong *et al*. (2017) further conducted research on concrete-filled steel tubular columns with high-strength materials under different loading conditions. Apart from the structural members, Coelho and Bijlaard (2007) firstly investigated the behaviour of steel beam-to-column joints with endplates being fabricated from high-strength materials. The connection method, endplate thickness and type of high-strength bolt were the varied test parameters. Afterwards, Qiang *et al*. (2014, 2015) extended the research to examine the performance of beam-to-column joints under and after fire conditions. Similarly, high-strength material was only used for the endplates, rather than the whole structural steel members. Oh and Park (2016) reported a series of experimental results of seven welded beam-to-column joints with HSS. The steel beams and columns were fabricated from high-performance materials with the yield stress up to 750 MPa. The effects of various reinforcing stiffeners in beam flanges on the deformation capacity of the connection under cyclic loading were investigated.

The above literature review demonstrates that studies on bolted HSS beam-to-column joints have not been carried out sufficiently. This paper thus presents finite element models using ABAQUS (2016) for predicting the behaviour of beam-to-column joints with high-strength materials. The accuracy and applicability of the developed numerical model are validated against independent experimental results. Extensive parametric studies are thereafter conducted to examine the effects of key design parameters on the HSS bolted beam-to-column joints under monotonic loading. The recorded moment-rotation curves from numerical models are utilised to characterise the mechanical performance of these connections. In addition, the initial stiffness, flexural resistance and ductility of these connections are further compared with those provided by the codes of practice. Design recommendations are then provided for HSS double extended endplate beam-to-column joints.

2. Finite element analysis

2.1 Basic concept

Field-testing is the most reliable method to study the behaviour of high-strength steel beam-to-column joints. However, the actual tests are time-consuming and expensive to examine the effects of every parameter on the behaviour of the connections. Moreover, the satisfactory results produced by finite element analysis have been demonstrated by previous studies (Shi *et al*. 2008, Wang *et al*. 2018). Therefore, the research present herein also proposes finite element models based on ABAQUS (2016) to extend the experimental database. The corresponding design recommendations for HSS beam-to-column joints are thereafter provided based on the obtained numerical analysis results.

An accurate finite element model is developed using ABAQUS/Explicit to simulate the performance of steel beam-to-column joints. Unlike the implicit method, the explicit method can easily overcome numerical convergence issues encountered in the implicit method due to large deformation and contact problems. Detailed guidance on the use of ABAQUS/Explicit is provided by Thai *et al*. (2017).

2.2 Finite element model

In the developed finite element models for bolted steel beam-to-column joints, the endplates, steel columns and beams are modelled using 8-node linear brick elements with reduced integration (C3D8R). The accuracy and benefits of

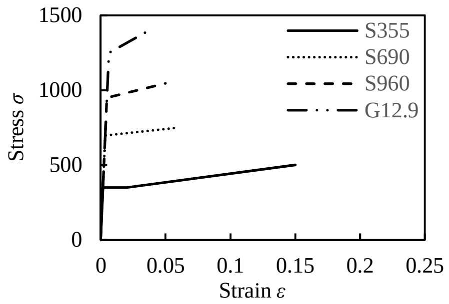

Fig. 2 Material properties for various steel components

using reduced integration elements have also been demonstrated by Augusto *et al*. (2016). For high-strength structural bolts, an eight-node quadratic brick element with reduced integration (C3D8R) is chosen owing to their ability to capture stress concentration more effectively (Li *et al*. 2016a). Moreover, structural bolts are modelled as merged components as the threads stripping is not observed. In this analysis, a mesh convergence study is conducted to provide a rational mesh size, which secures the accuracy of the model with the least computational time.

Both ends of the steel column are constrained by the fixed-ended boundary conditions. The axial compressive load is applied on top of the column through a pre-defined reference point to simulate a service load. Another vertical load is applied to the end of the steel beam with displacement control.

Surface-to-surface contact with a Hard Contact Model in the normal direction with no penetration is considered for all contact surfaces. A Coulomb friction model in the tangential direction is assumed with a friction coefficient. The appropriate value of the friction coefficient depends on the surface treatment (Li *et al*. 2016b). As suggested by Vasdravellis *et al*. (2009), Vasdravellis and Uy (2014), the frictional coefficient is taken as 0.25 between the steel components with cleaned surfaces. The contact surfaces of the bolted steel beam-to-column joints are the inner surface of the endplate to the outer surface of the steel column, the bolt head to the endplate and the bolt nut to the column flange, as well as the bolt shank to the bolt hole. Apart from the contact interactions, "Tie" constraint is employed to simulate the welding between endplates and steel beams. For welded steel beam-to-column joints, only the "Tie" constraint is utilised to simulate the connections between steel beams and columns, which has been demonstrated by Sabbagh *et al*. (2013) and Xu *et al*. (2017).

Table 2 Structural steel for fracture simulation

Steel	D_1	D_2	D_3
S355	0.036	0.069	-0.5
S690	0.030	0.015	-0.5
S960	0.029	0.012	-0.5
G12.9 bolt	0.025	0.03	-0.5

The material property of the structural steel, including the beam and column section, endplate and high-strength bolt, has to be carefully considered in the developed finite element model. For the model verification purposes, the inelastic behaviour of structural steel is modelled using a multi-linear elastic-plastic model based on the reported results, as shown in Fig. 2. The nominal yield and ultimate stress of these structural steel members are listed in Table 1. Furthermore, to capture the fracture behaviour of structural steels, damage model proposed by Johnson and Cook (1985) is used. Since the dimensionless strain rate and homologous temperature is not considered in this study, Li *et al*. (2018) simplified this method and the damage initiation is determined through Eq. (1)

$$\varepsilon_f = D_1 + D_2 \exp(D_3 \eta) \tag{1}$$

where ε_f is the equivalent strain to fracture, and the dimensionless pressure-stress ratio is defined as $\eta = \sigma_m/\sigma$, where σ_m and σ is the average of three normal stresses and von Mises equivalent stress, respectively. D_1, D_2 and D_3 are material dependent fracture constants, as summarised in Table 2.

3. Verifications of the numerical analysis

In order to validate the accuracy and applicability of the developed numerical model, four beam-to-column joints with high-strength materials as part of the connections are selected for comparison. In particular, these specimens are bolted beam-to-column joints and are subjected to monotonic loading, which is reported by Coelho and Bijlaard (2007). The detailed descriptions of the selected specimens are presented in the following sections.

3.1 Description of the selected specimens

In this study, four specimens from the experimental program that were tested by Coelho and Bijlaard (2007) are

Table 1 Summary of selected specimens: utilised members and material properties

Specimens	Beam	Column	Endplate				Bolt				References
			Type	Thickness (mm)	f_y (MPa)	f_u (MPa)	ϕ_b (mm)	Grade	f_y (MPa)	f_u (MPa)	
F1EP-10-2	HE320A for beam; HE300M for column (S355) f_y = 345 MPa f_u = 500 MPa		FEP (S690)	10	698	750	24	12.9	1250	1413	Coelho and Bijlaard (2007)
F2EP-15-2				15	774	815	24	12.9	1250	1413	
EEP-10-3			EEP (S690&S960)	10	952	1046	24	12.9	1250	1413	
EEP-15-2				15	774	815	24	12.9	1250	1413	

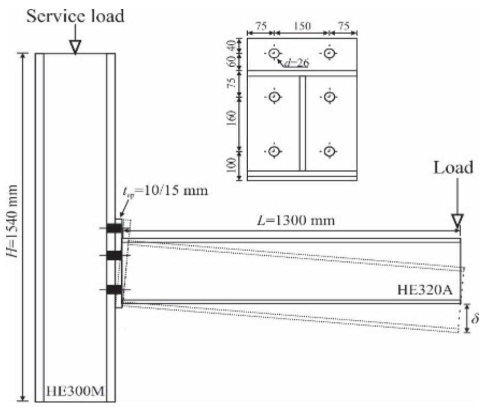

Fig. 3 Geometric details of the selected specimens

selected to validate the accuracy of the finite element model. All specimens consist of a HE320A beam section with a length of 1300 mm and a relatively larger HE300M section as the connected column. The test specimens differ in design details, such as the use of flush endplate and extended endplate, as well as the thickness of these endplates. Specifically, both specimens F1EP-10-2 and F2EP-15-2 utilise flush endplates but differ in endplate thickness. Another two specimens EEP-10-3 and EEP-15-2 connect the steel beams to the columns though extended endplates. The thickness of the extended endplates is also a design parameter under investigation. The geometric details of the specimens are illustrated in Fig. 3. During the test, the columns are constrained at both ends, whilst a monotonic compressive loading is applied at the tip of the steel beam vertically. The material properties of the specimens are shown in Table 1.

3.2 Comparisons of the failure modes

To assess the accuracy of the developed numerical model, comparisons of the failure modes between the experimental and finite element analysis results are carried out. As stated by Coelho and Bijlaard (2007), the specimens with 15 mm thick endplates failed due to the fracture of bolts in tension. This phenomenon occurred prior to the full development of the yield line in the endplates. Figs. 4(a) and (b) presents the final state and failure modes of the selected specimen. On the contrary, for the specimens with endplates of 10 mm thickness, the failure of welding between the endplates and attached beam was observed prior to the fracture of bolts (Fig. 4(c)). This failure mode provides more ductile behaviour and larger rotational capacity for the beam-to-column joint. As can be seen, the developed finite element model is accurate and can predict the failure modes that are close to the test specimens.

3.3 Comparisons of moment-rotation curves

In addition to the final state failure modes, comparisons of the moment-rotation (M-ϕ) curves between experiment and finite element analysis further demonstrate the accuracy of the developed numerical model. The vertical displacement and reaction force response at the tip of the steel beam is recorded by ABAQUS. The M-ϕ relationships of the connections under monotonic loading are plotted with the recorded results. Specimens F2EP-15-2 and EEP-15-2 utilise 15 mm thick endplates between the steel columns and beams. Due to the poor rotational capacity, both specimens fail with the bolt fracture. On the contrary, specimens F1EP-10-2 and EEP-10-3 with 10 mm thick endplates exhibit more ductile performance, and fail by the welding fracture. Moreover, compared with the specimens with flush endplates (F1EP-10-2 and F2EP-15-2), their counterparts with extended endplates show more rotational capacities, which can be observed in Fig. 5. It can be seen that the stiffness and ultimate strength of the steel beam-to-column joints obtained from the finite element model agree

(a) With specimen F2EP-15-2

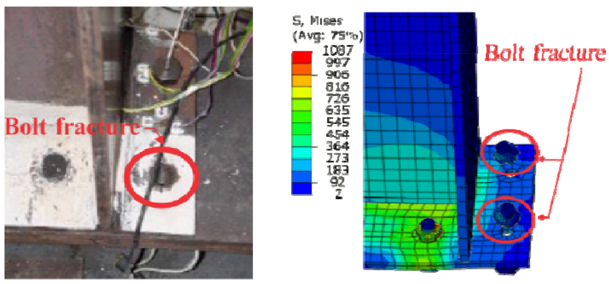

(b) With specimen EEP-15-2

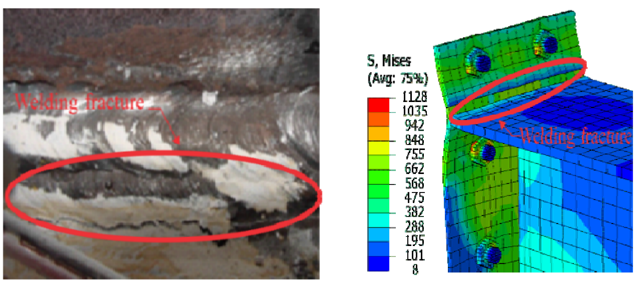

(c) With specimen EEP-10-3

Fig. 4 Failure mode comparisons of the specimens selected from Coelho and Bijlaard (2007)

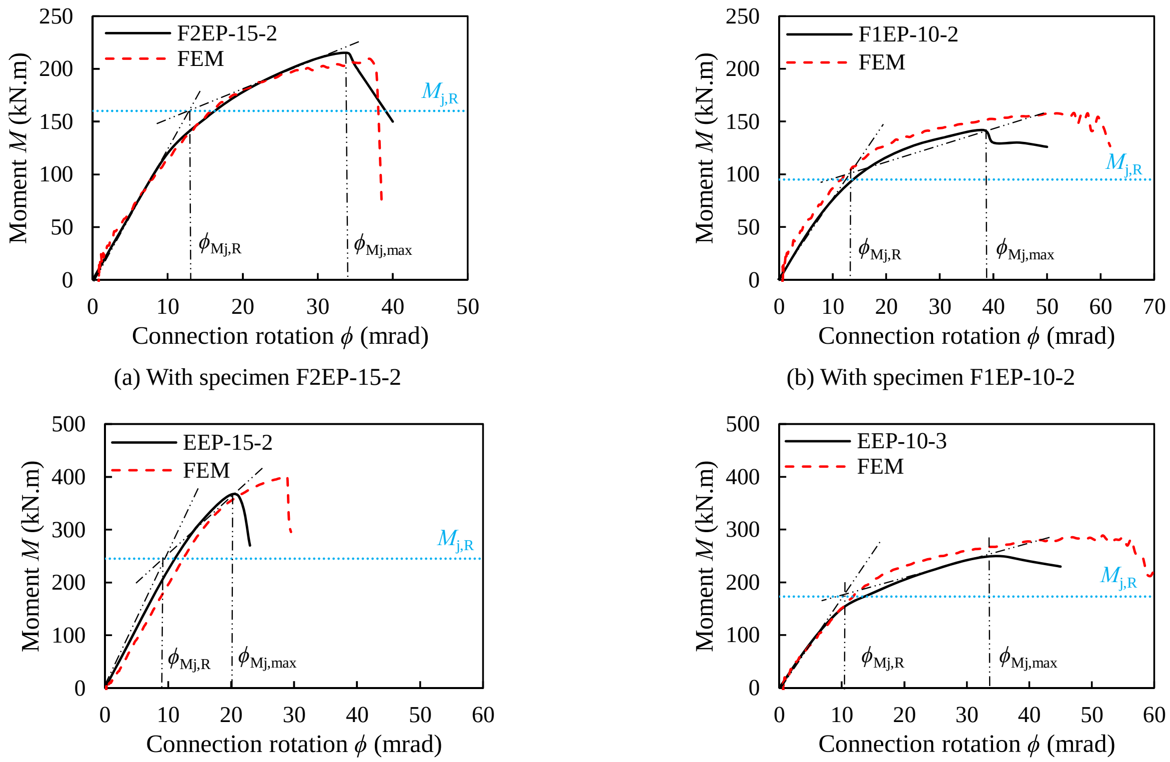

(a) With specimen F2EP-15-2 (b) With specimen F1EP-10-2

(c) With specimen EEP-15-2 (d) With specimen EEP-10-3

Fig. 5 Validation of finite element models for high strength steel beam-to-column joints

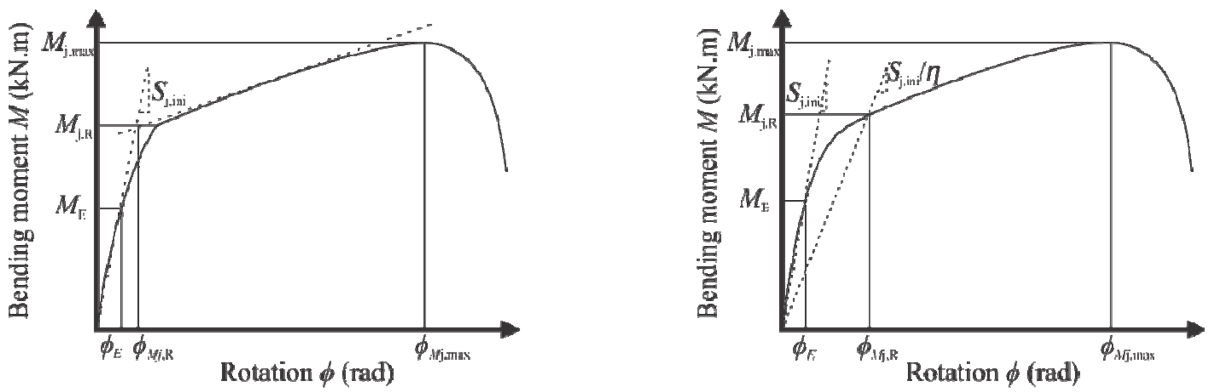

(a) Defined by Zanon and Zandonini (1988) (b) Defined by Weynand (1997)

Fig. 6 Moment-rotation curve with different plastic flexural resistance

well with that from the experimental study. The post-peak behaviour of the connections is simulated reasonably accurately.

4. Numerical analysis for joints with various design methods

4.1 Moment-rotation curve

Typical moment-rotation (M–ϕ) curves for bolted steel beam-to-column joints are illustrated in Fig. 6, where the main characteristics of the beam-to-column joints can be obtained. In these curves, M and ϕ represent the applied bending moment and the joint rotation, respectively. The applied moment can be calculated as the product of the applied vertical load and the distance from this loading point to the surface of the column.

$$M = P \times L \tag{2}$$

Normally, a bolted steel beam-to-column joint rotation is constituted by the rotation of the connection (such as the endplate and bolt) and the rotation of the panel zone of the column web. Particularly, the connection rotation is defined as rotation between the centrelines of connected steel column and beam

$$\phi = \theta_b - \theta_c \tag{3}$$

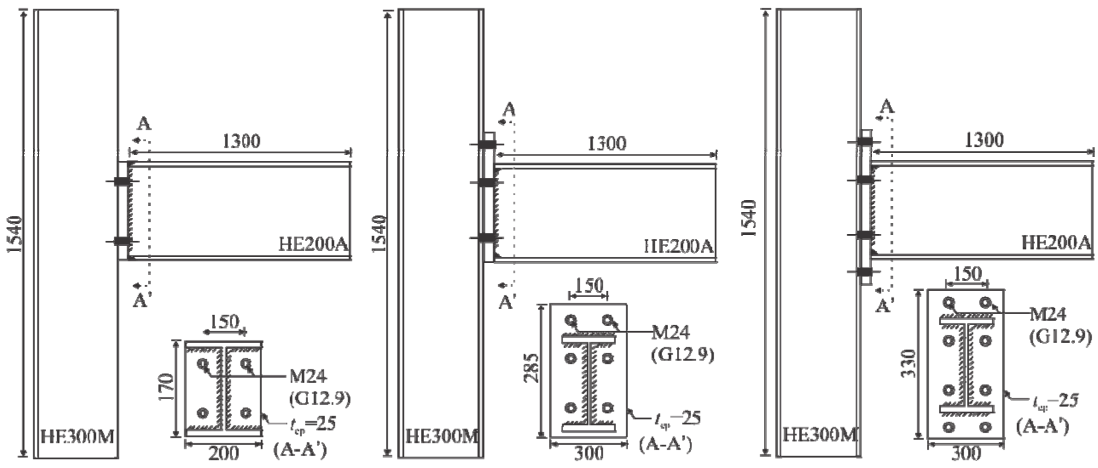

Fig. 7 Geometric details of different beam-to-column joints

where θ_b and θ_c is the rotation of the steel beam and column, respectively. In the present study, the specimens selected as validation consist of relatively stiffer steel columns, which indicates minor deformation of the columns and panel zones can be observed. The total joint rotation is thereafter determined as the beam rotation only. From these moment-rotation curves, the elastic moment (M_e), the plastic flexural moment resistance ($M_{j,R}$) and the ultimate moment capacity ($M_{j,max}$) can be obtained. Correspondingly, the rotation of the beam-to-column joint at the elastic moment (ϕ_e), plastic flexural moment ($\phi_{Mj,R}$) and ultimate moment ($\phi_{Mj,max}$) can also be determined.

As observed in Fig. 6(a), Zanon and Zandonini (1988) defined the plastic flexural moment ($M_{j,R}$) at the point where the initial stiffness and the post-limit stiffness intersects. Alternatively, Weynand (1997) determined the plastic moment ($M_{j,R}$) by using a secant stiffness, which can be obtained by dividing the initial stiffness with a fixed coefficient η, as shown in Fig. 6(b). In the latter method, the secant stiffness is small. Considering the relatively smaller rotational capacities of the high-strength steel beam-to-column joints, it is difficult to locate the plastic flexural moment during the ascending branch of the M–ϕ curves. Thus, the former method for determining the plastic flexural moment, which largely relies on the determination of the post-limit stiffness is adopted in the present analysis.

4.2 Various connection methods

This paper analyses the behaviour of different types of steel beam-to-column joints through finite element model. The connections are designed with various failure modes occurred in the connection regions. Specifically, the steel column used herein is HE300M with a length of 1540 mm, which is a relatively stiffer member. Meanwhile, a smaller steel section HE200A is used as a beam member with a plastic moment of 270 kN.m. The geometric details of these connections are illustrated in Fig. 7. The yield strength and ultimate strength of the HSS utilised is 690 MPa and 750 MPa, respectively. The high-strength bolts utilised for the following FE models are Grade 12.9 M24.

The moment-rotation curves of these three different beam-to-column joints are compared in Fig. 8. It can be seen from Fig. 8 that these connections can be categorised as semi-rigid and partial-strength connections according to the current design provision EC3-1-8 (2005). The ultimate moment resisting capacities of connections with flush endplates and extended endplates differ significantly. The beam-to-column joint with double extended endplate (DEEP) show the similar behaviour to the connection with single extended endplate (SEEP). On the contrary, the beam-to-column joint with flush endplate (FEP) shows the lowest ultimate moment resisting capacity and the lowest initial stiffness. Moreover, the beam-to-column joint with flush endplate undergo a sudden drop in moment resistance owing to the bolt fracture, which is different from the other two connections. The failure mode of connection with single extended endplate is similar to that of connection with the double extended endplate. The failure modes of selected connections are shown in Fig. 9.

The higher moment resisting capacity of connection with extended endplate is due to the increased lever arm between the compressive forces and the tensile forces in the connection regions. In addition to the higher moment capacity and initial stiffness, the better performance in terms of seismic resisting also renders the beam-to-column joint with DEEP ideal for design purposes. Thereafter, the following numerical analysis is carried out based on this type of connection.

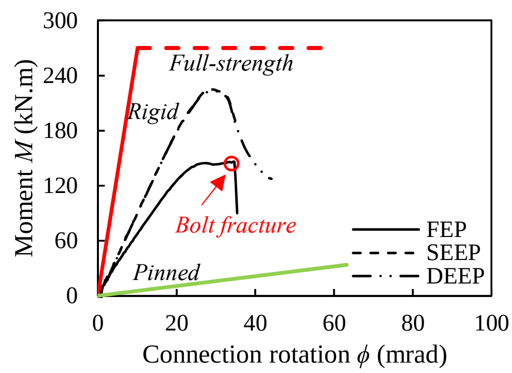

Fig. 8 Comparison of moment-rotation curves for different connections

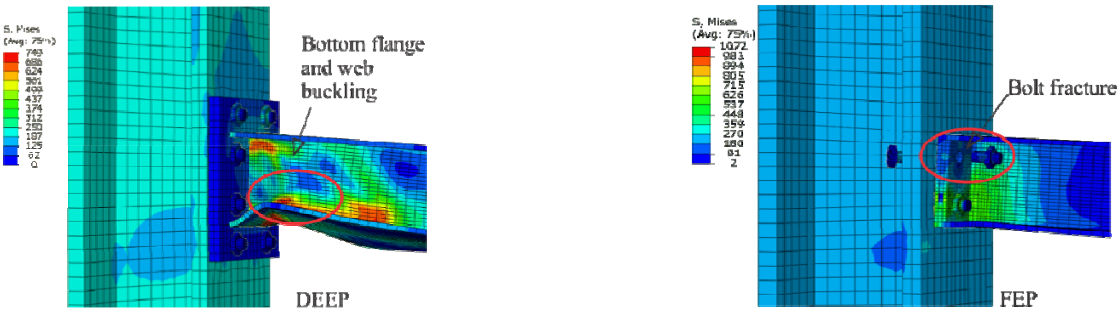

(a) With DEEP (b) With FEP

Fig. 9 Failure modes of beam-to-column joints

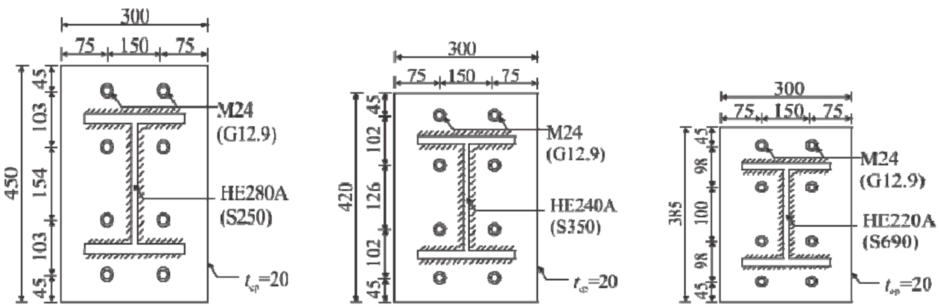

Fig. 10 Details of connection regions with various steel beams

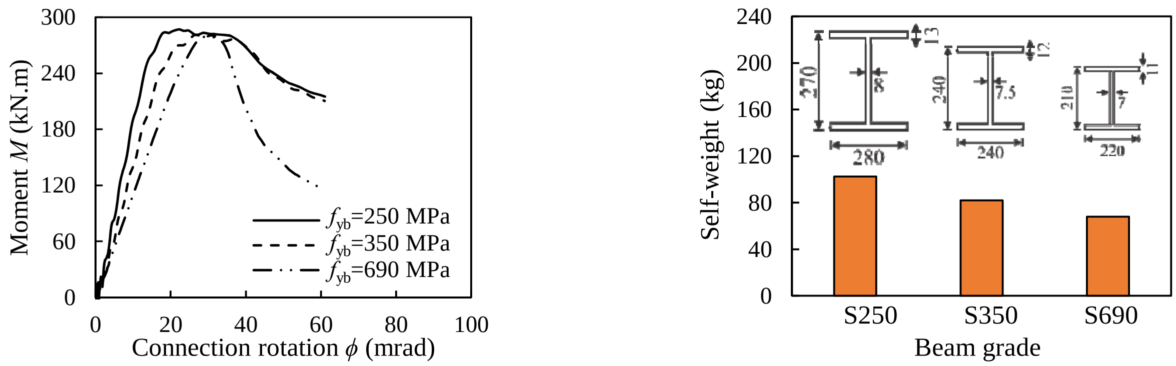

(a) Moment-rotation curves (b) Self-weight of the steel beams

Fig. 11 Benefits of using HSS in beam-to-column joints

4.3 Benefits of using high-strength steel

The present analysis investigates the benefits of using high-strength steel in beam-to-column joints. The analysis herein simply fixes the column section size and the benefits of using high-strength materials are only examined by varying the steel beam sections. For comparison purposes, the plastic moment resisting capacities of the steel beams are kept as similar as possible. The connections are designed with the full plastic moment developed in the steel beams, rather than the failure occurred within the connection regions. The details of connection regions are illustrated in Fig. 10, which mainly include the dimensions of the endplates, as well as the distances between bolts and endplate edges. In addition, the steel columns are kept as HE300M with a length of 1540 mm. The beam section HE280A and HE220A are chosen for steel beams with steel grade of S250 and S690, respectively. For steel beam with a grade of S350, slightly modification based on the beam section HE240A is conducted and utilised. The geometric details of these steel beams of various steel yield stresses are shown in Fig. 11(b).

The moment-rotation curves of these connections are compared in Fig. 11(a) and it is shown that these connections possess similar ultimate moment resistances. The most significant benefit of using high-strength steel (S690) as steel beam in beam-to-column joint is then presented in Fig. 11(b). With the similar moment capacity, the self-weight of the steel beam of high-strength steel (S690) can be 40% lower than that of the beam with mild steel (S250). Again, the reduced section sizes and lowered self-weight of the structural elements encourage the wide application of this high-performance material. It is worth noting that the decreased initial stiffness for connection

Table 3 Geometric information of specimens for parametric study

Group	No.	Bolt		Endplate		Column
		Grade	Pretension f_{pt}/f_{ub}	Thickness t_{ep} (mm)	Yield stress $f_{y,ep}$ (MPa)	$b_f \times h \times t_f \times t_w$ (mm)
C1	FE1	10.9	0	15	690	310×340×39×21
a	FE2	**8.8**	0	15	690	310×340×39×21
	FE3	**12.9**	0	15	690	310×340×39×21
b	FE4	10.9	**0.2**	15	690	310×340×39×21
	FE5	10.9	**0.4**	15	690	310×340×39×21
c	FE6	10.9	0	**10**	690	310×340×39×21
	FE7	10.9	0	**20**	690	310×340×39×21
d	FE8	10.9	0	15	**960**	310×340×39×21
	FE9	10.9	0	15	**350**	310×340×39×21
	FE10	10.9	0	15	**250**	310×340×39×21
e	FE11	10.9	0	15	690	226×240×**15**×21
	FE12	10.9	0	15	690	226×240×**22**×21
	FE13	10.9	0	15	690	226×240×**30**×21
C2	FE14	10.9	0	15	690	226×240×39×21
f	FE15	10.9	0	15	690	226×240×39×**30**
	FE16	10.9	0	15	690	226×240×39×**15**
	FE17	10.9	0	15	690	226×240×39×**10**

Table 4 Summary of material properties for various structural steels

Structural steels	Young's moduls E_s (GPa)	Yield stress or 0.2% proof stress f_y or $f_{0.2\%}$ (MPa)	Ultimate stress f_u (MPa)
Bolt (Grade 8.8)	200	640	800
Bolt (Grade 10.9)	200	936	1040
Bolt (Grade 12.9)	200	1080	1200
Steel (S250)	200	250	420
Steel (S350)	200	350	520
Steel (S690)	200	690	760
Steel (S960)	200	960	1040

with high-strength steel beam is due to the decreased lever arm between the bolts in compression and tension.

4.4 Parametric studies for double extended endplate connections

This paper attempts to enhance the understanding of the behaviour of steel beam-to-column joints with high-strength materials through extensive parametric studies. These extensive numerical analysis results also provide additional information for the limited experimental database. The authors herein take into account six design parameters, which are highlighted in Table 3. A series of analyses are conducted with one parameter varied each time accordingly. In the following numerical analysis, two control specimens are used. Specimens C1 is the first control specimen with HE300M as the steel column, which is used for the comparisons with those in Groups a-d. The purpose of using a stiffer column section is to assure the effects of steel column on the connection behaviour can be minimised. The second control specimen (C2) utilises smaller steel column section HE220M, which could render the effects of column flange and web thickness on the connection behaviour more obvious. In addition to the geometric details of the specimens used in finite element analysis, the material properties of each structural steel with nominal values are summarised and listed in Table 4.

4.4.1 Effects of bolt grade

In this analysis, the structural bolts with different grades are used to investigate the influences on the moment-rotation curves of the steel beam-to-column joints. The most common structural bolts used in the construction industry are limited to Grade 8.8. However, with the higher strength steel used in the building structures, the application of higher grade structural bolts becomes necessary. In the

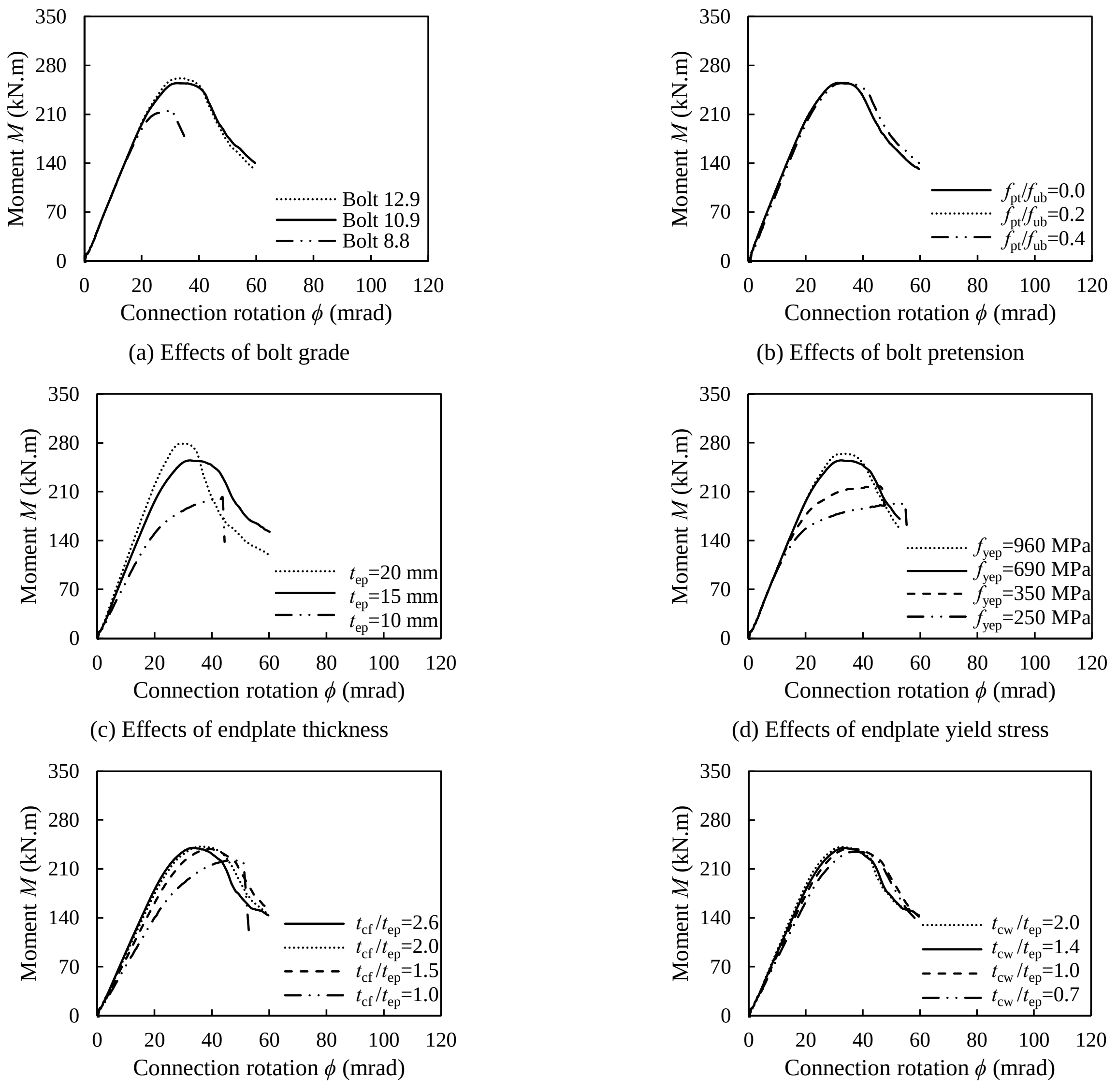

(a) Effects of bolt grade (b) Effects of bolt pretension

(c) Effects of endplate thickness (d) Effects of endplate yield stress

(e) Effects of column flange thickness (f) Effects of column web thickness

Fig. 12 Effects of various design parameters on moment-rotation cuves

current market, structural bolts of grade 10.9 and grade 12.9 could be the alternative. As shown in Fig. 12(a), the use of higher grade structural bolts can improve the ultimate moment resistance of the connections. Particularly, the use of structural bolts with Grade 8.8 leads to a brittle failure, where the fracture of bolts in the tension side can be observed. Compared to the beam-to-column joint with Grade 10.9 bolt, the behaviour of the connection with higher bolt grade (12.9) does not show too much strength and initial stiffness improvement. These phenomena are to be expected, as the initial stiffness from the bolts largely relies on the bolt length, rather than the bolt strength or grade. Moreover, the specimens FE1 and FE3 consist of smaller beam sections.

4.4.2 Effects of bolt pretension

Currently, bolt pretension is a common engineering practice that is particularly used for structural bolts with higher strength grade. Appropriate bolt pretension can improve the reliability and fatigue performance of the connection. Generally, the bolt pretension can be characterised by the tightening torque, which is calculated as following

$$M_{PT} = KP_0D \tag{4}$$

where K is the tightening coefficient and normally ranged between 0.1 to 0.2, depends on the treatment of the surface; P_0 and D is the tightening force and diameter of the pre-tensioned bolt. To analyse the effects of bolt pretension on the behaviour of the connections, this parameter is generalised as a ratio of applied pretension stress to the bolt ultimate stress (f_{pt}/f_{ub}). Three levels of bolt pretension are taken into consideration in this analysis, which include f_{pt}/f_{ub} = 0.0, 0.2 and 0.4. As shown in Fig. 12(b), the level of bolt pretension has limited effects on the moment-rotation curves of the connections. The initial stiffness of the connections is not affected when increasing the bolt pretension to 20% of its ultimate stress, which is the normally applied bolt prestress. This is to be expected since the stiffness of the bolt is relevant to the bolt length rather than the bolt stress. However, an earlier failure can be expected with high bolt pretension when the failure mode of the connection is governed by the bolt fracture.

4.4.3 Effects of endplate thickness

Three different endplate thickness are used in this study which included t_{ep} = 10, 15 and 20 mm. It is shown in Fig. 12(c) that increasing the endplate thickness can increase the initial stiffness and ultimate moment capacities of the connections. For connections with thick endplates, the deformation of endplates is limited, which results in smaller rotation of the connections. On the contrary, relatively larger connection rotation can be observed when decreasing the endplate thickness. For design purposes, the upper limit of endplate thickness can be regarded as the point where the ductility requirement is just satisfied (ϕ_{max} = 30 mrad), so that the sacrifice of strength and stiffness is not significant. On the other hand, the lower limit of endplate thickness can be set as the point where deflection of the steel beam can satisfy the service loading requirement.

4.4.4 Effects of endplate yield stress

Connections FE1 and FE8 to FE10 in Table 3 are used to evaluate the influence of the endplate yield stress on the mechanical performance of the high-strength steel beam-to-column joints. As illustrated in Fig. 12(d), utilising endplates with higher strength grade can increase the ultimate moment capacities of the connections. The ultimate moment resistance is enhanced by 30% when replacing the grade S250 steel endplate with grade S690 steel endplate. Similar to the effects of endplate thickness, the lower the endplate yield stress is, the larger the connection rotation will be. For the connections with endplates fabricated from mild steel, large rotation of the beam-to-column joints over 40 mrad can be observed, which directly induce the bolt fracture. Nevertheless, keep increasing the endplate yield stress cannot always lead to a higher moment capacity of the connection. This phenomenon is mainly attributed to the fact that the critical component of the connection is changed to the steel beams when the strength of the endplates reached a certain level.

4.4.5 Effects of column flange thickness

In a single sided steel bolted beam-to-column joint with double extended endplate, the components to be considered are the column web panel in shear, the column web in compression and tension, the column flange and endplate in bending, as well as the bolts in tension. In the previous numerical analysis, the steel column is designed with large section, which means the effects of column flange and web can be minimised when considering the effects of other design parameters. However, the effects of column flange and column web thickness need to be investigated in the following study. Thus a smaller steel section HE240M is chosen to replace the original HE300M column section. The effects of column flange thickness are generalised as a ratio of column flange thickness to endplate thickness (t_{cf}/t_{ep}). As illustrated in Fig. 12(e), increasing the ratio of t_{cf}/t_{ep} leads to a stiffer steel column section, the initial stiffness and ultimate moment capacity can therefore be increased.

4.4.6 Effects of column web thickness

Similar to the column flange thickness, the column web thickness is generalised as a ratio to the endplate thickness (t_{cw}/t_{ep}). In order to investigate the effects of column web thickness on the moment-rotation curves of the bolted beam-to-column joints, four different ratios (t_{cw}/t_{ep}) were used. It can be observed in Fig. 12(f) that the effects of column web thickness on the steel beam-to-column joint are limited, although it showed a trend that increasing the column web thickness can increase the initial stiffness and moment capacity of the connections.

5. Comparisons with Eurocode 3 and discussion

The current design provisions for high-strength steel beam-to-column joints (EC3-1-12, 2007) does not allow the semi-continuous or the partially-restrained concept to be used. The connections with high-strength materials have to be designed based on the elastic distribution of forces. However, according to the experimental results obtained from Coelho and Bijlaard (2007) and the numerical results in the present study, it can be seen that most of the specimens with high-strength materials can also exhibit sufficient rotational capacities and ductility. Therefore, comparisons between the experimental, numerical results and current codes of practice (EC3-1-8, Eurocode 2005) in terms of the plastic flexural moment capacities, initial stiffness and ductility are carried out. It should be noted that the actual and nominal material characteristics are used for the experimental and numerical specimens, respectively. Partial safety factors are taken as unitary.

5.1 Plastic flexural resistance

As indicated by the EC3-1-8 (2005), the steel beam-to-column joints transmit the applied moments through a series of structural components. The plastic flexural moment that a particular joint can resist is calculated through Eq. (5)

$$M_{j.Rd} = \sum_{i=1}^{n} F_{ti.Rd} h_i \tag{5}$$

where $F_{ti.Rd}$ represents the tensile resistance of bolt row i and h_i represents the distance between the i^{th} bolt row to the

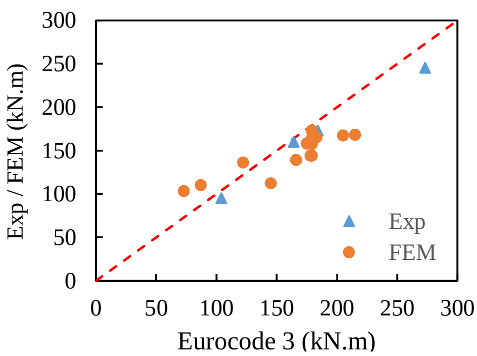

Fig. 13 Comparisons of moment capacity between experiment, FEM and EC3

Table 5 Summary of the moment resisting capacities of the specimens

Specimens	Experimental			FEM			Eurocode 3	$M_{j,R,exp}$ / $M_{j,R,EC3}$ or $M_{j,R,FEM}$ / $M_{j,R,EC3}$
	$M_{j,E,exp}$ (kN.m)	$M_{j,R,exp}$ (kN.m)	$M_{j,max,exp}$ (kN.m)	$M_{j,E,FEM}$ (kN.m)	$M_{j,R,FEM}$ (kN.m)	$M_{j,max}$ (kN.m)	$M_{j,R,EC3}$ (kN.m)	
F1EP-10-2	63	95	142	-	-	-	104	0.91
F2EP-15-2	107	160	215	-	-	-	164	0.98
EEP-10-3	115	173	244	-	-	-	184	0.94
EEP-15-2	163	245	366	-	-	-	273	0.90
FE1	-	-	-	105	158	254	175	0.90
FE2	-	-	-	75	112	216	145	0.77
FE3	-	-	-	111	167	261	205	0.81
FE4	-	-	-	105	158	254	175	0.90
FE5	-	-	-	105	158	254	175	0.90
FE6	-	-	-	81	110	200	87	1.26
FE7	-	-	-	110	165	280	183	0.90
FE8	-	-	-	112	168	263	215	0.78
FE9	-	-	-	91	136	217	122	1.11
FE10	-	-	-	69	103	193	73	1.41
FE11	-	-	-	93	139	222	166	0.84
FE12	-	-	-	96	144	238	179	0.80
FE13	-	-	-	105	158	240	179	0.88
FE14	-	-	-	109	164	240	179	0.92
FE15	-	-	-	115	173	241	179	0.97
FE16	-	-	-	105	157	239	179	0.88
FE17	-	-	-	96	144	233	178	0.81
Mean								0.93
SD								0.15

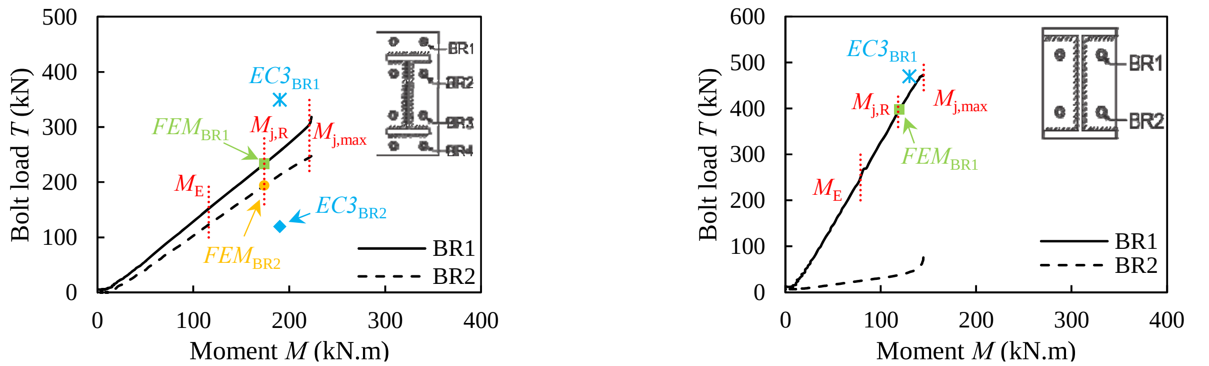

(a) With DEEP (b) With FEP

Fig. 14 Comparisons of bolt forces with design codes for different beam-to-column joints

centre of the compression.

As can be observed in Table 5 and Fig. 13, the plastic flexural moment capacities of most of the specimens are overestimated by the EC3-1-8 (2005). Only three specimens in the numerical analysis, where large plastic deformation of endplates occurred, show higher plastic flexural moment capacities than those predicted by the design provisions. This phenomenon indicates that the current design code is unsafe for the design of high-strength steel bolted beam-to-column joints. Some modifications might be necessary to ensure the applicability of the current design provisions to the beam-to-column joints with high performance materials.

5.2 Bolt forces in different beam-to-column joints

As bolts play important roles in determining the strength of the steel beam-to-column joints, the tensile strength in the bolts from the finite element models is recorded. These recorded bolt tensile forces are further compared with the equivalent tensile resistance at each bolt row $F_{\mathrm{ti,Rd}}$, as shown in Fig. 14. It is worth noting that the bolt tensile force is only recorded for a single bolt in a particular row, thus the equivalent tensile resistance at each bolt row $F_{\mathrm{ti,Rd}}$ is taken as half of the calculated value based on the EC3-1-8 (Eurocode 2005). Moreover, the numerical analysis in section 4.4 utilise similar design details at the connection regions. Therefore, the specimens in Section 4.2 with different connection design methods are used herein for analysis.

It can be seen from Fig. 14 that the bolts in row 1 (BR 1) show slightly higher tensile force development than that in bolt row 2 (BR2), which is coherent with the analytical method in EC3-1-8 (2005), but different from the results reported by Abidelah *et al*. (2012). This phenomenon is mainly attributed to the thickness of endplates used in different studies. The beam-to-column joints used in this section include 25 mm thick endplates, while the specimens tested by Abidelah *et al*. (2012) involved endplates of 15 mm thickness. The stiffer endplates lead to less plastic deformation of the connection regions, which in turn results in higher tensile forces developed in the bolts at the upper level (BR1).

Table 6 Summary of the initial stiffness and rotation capacities of the specimens

Specimens	Exp $S_{\mathrm{j,ini,\,exp}}$ (kN.m/mrad)	FEM $S_{\mathrm{j,ini,FEM}}$ (kN.m/mrad)	EC3 $S_{\mathrm{j,ini,EC3}}$ (kN.m/mrad)	$S_{\mathrm{j,R,exp}}$ / $S_{\mathrm{j,R,EC3}}$ or $S_{\mathrm{j,R,FEM}}$ / $S_{\mathrm{j,R,EC3}}$
F1EP-10-2	7.8	-	10.3	0.76
F2EP-15-2	12.3	-	20.6	0.60
EEP-10-3	17.2	-	20.5	0.84
EEP-15-2	35.3	-	39.4	0.90
FE1	-	13.1	19.5	0.67
FE2	-	13.1	19.5	0.67
FE3	-	13.1	19.5	0.67
FE4	-	13.1	19.5	0.67
FE5	-	13.1	19.5	0.67
FE6	-	8.8	9.7	0.91
FE7	-	19.2	25.7	0.75
FE8	-	13.1	18.3	0.72
FE9	-	13.1	18.3	0.72
FE10	-	13.1	18.3	0.72
FE11	-	15.3	19.8	0.77
FE12	-	15.6	23.3	0.67
FE13	-	16.7	24.7	0.68
FE14	-	17.3	24.8	0.70
FE15	-	18.1	27.3	0.66
FE16	-	15.0	20.2	0.74
FE17	-	12.1	15.3	0.79
Mean				0.73
SD				0.08

The beam-to-column joint with double-extended endplate shown in Fig. 14(a) does not fail with the bolt fracture. The critical component is the bottom flange of steel beam under compression. Therefore, the recorded bolt tensile forces could not match with the predicted equivalent tensile resistance at each bolt row. Specifically, the equivalent tensile resistance at bolt row 1 (BR1) is dominated by the tensile capacity of the endplate in bending, which is higher than the tensile forces in the bolts at BR1.

On the contrary, the beam-to-column joint with flush endplate shown in Fig. 14(b) fails suddenly with bolt fracture at the upper level (BR1). The bolts at the lower level (BR2) does not exhibit tensile resistance until the maximum moment is reached. Comparison in terms of the bolt tensile forces between the numerical analysis and EC3-1-8 (2005) is conducted. As can be seen, the bolt tensile forces predicted by the current codes of practice is close but slightly higher than the numerical result. This small discrepancy indicates the current analytical method needs to be modified for predicting the strength of high-strength steel beam-to-column joint with the flush endplate.

5.3 Initial stiffness

The initial stiffness of the specimens is computed with Eq. (6) that is given in EC3-1-8 (2005).

$$S_{j,ini} = Ez^2 \Big/ \sum_i 1/K_i \qquad (6)$$

In Eq. (6), z is the lever arm taken equal to the distance from the centre of compression to a point midway between the two bolt-rows in tension and k_{i} is the stiffness coefficients for joint component i. The stiffness coefficients that have to be taken into account are column web in shear (k_1), column web in compression (k_2) and the equivalent stiffness coefficient related to the bolt-rows in tension (k_{eq}), which is evaluated using Eqs. (7) and (8).

$$K_{eq} = \frac{\sum_r k_{eff,r} h_r}{z} \qquad (7)$$

$$k_{eff,r} = \frac{1}{\sum_i 1/k_{i,r}} \qquad (8)$$

It is shown in Table 6 and Fig. 15 that the initial stiffness of the specimens from the experimental tests and numerical analysis are smaller than those predicted by the codes of practice. According to the current method, the initial stiffness of the high-strength steel bolted beam-to-column joints can be overestimated by 25%. Furthermore, it can be observed that the double-extended endplate with larger thickness can significantly enhance the initial stiffness of the connections. Similarly, the column flange and web thickness can also proportionally affect the initial stiffness of the bolted beam-to-column joints.

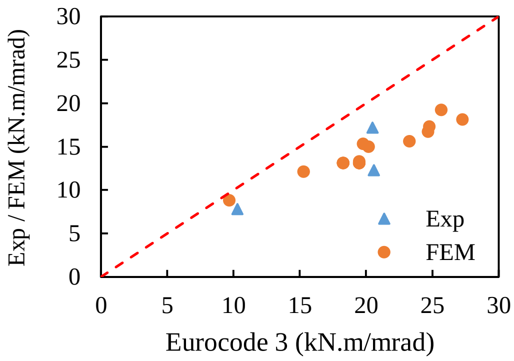

Fig. 15 Comparisons of initial stiffness between experiment, FEM and EC3

Table 7 Summary of the rotation capacities and ductility of the specimens

Specimens	Experimental $\phi_{j,R,exp}$ (mrad)	Experimental $\phi_{j,max,exp}$ (mrad)	FEM $\phi_{j,R,FEM}$ (mrad)	FEM $\phi_{j,max,FEM}$ (mrad)	$\phi_{j,max,exp}/\phi_{j,R,exp}$ or $\phi_{j,max,FEM}/\phi_{j,R,FEM}$
F1EP-10-2	12.0	39.0	-	-	3.25
F2EP-15-2	13.0	33.0	-	-	2.54
EEP-10-3	10.0	36.0	-	-	3.60
EEP-15-2	7.0	20.0	-	-	2.86
FE1	-	-	14.0	34.7	2.48
FE2	-	-	7.8	30.0	3.85
FE3	-	-	14.3	35.4	2.48
FE4	-	-	14.0	32.4	2.31
FE5	-	-	14.0	32.4	2.31
FE6	-	-	12.1	43.7	3.61
FE7	-	-	11.1	29.2	2.63
FE8	-	-	14.3	32.8	2.29
FE9	-	-	10.0	45.4	4.54
FE10	-	-	7.6	52.8	6.95
FE11	-	-	14.9	46.0	3.09
FE12	-	-	15.6	38.1	2.44
FE13	-	-	16.0	34.1	2.13
FE14	-	-	16.1	34.1	2.12
FE15	-	-	17.2	32.0	1.86
FE16	-	-	15.8	34.0	2.15
FE17	-	-	14.3	35.6	2.49

5.4 Rotational capacity and ductility

Rotational capacity and ductility can be used to indicate the length of the yield plateau of the recorded moment-rotation curve for a particular steel beam-to-column joint. Specifically, for a bolted high-strength steel beam-to-column joint, the rotational capacity, together with the plastic flexural moment capacity and initial stiffness are of significant importance for designing a partial strength joint. Table 7 summarises the rotational capacities of a series of high-strength steel beam-to-column joints. As can be seen, the rotational capacities of connections can be significantly increased by (1) using thinner endplates; (2) using endplates with smaller steel yield stresses.

For conventional mild steel structures, a minimum 35-40 mrad plastic rotation is generally regarded as sufficient. Wilkinson *et al.* (2006) also suggested that a minimum rotation of 30 mrad has to be developed for beam-to-column joints in typical moment resisting frames, where seismic resisting is an important design criterion. As can be seen in Table 7, most of the specimens can satisfy this requirement except those with very thick endplates.

For the ease of calculation, the ductility of a beam-to-column joint is quantified with the adapted equation below

$$\upsilon_j = \frac{\phi_{j,\max}}{\phi_{j,R}} \tag{9}$$

The ductility index of these specimens are summarised in Table 6, with most of these ductility index values range from 2 to 3. As indicated by Coelho *et al.* (2006), a minimum ductility index value of 4.0 should be achieved for mild steel beam-to-column joints to avoid the brittle failure. If the same ductility index value is considered for the high-strength steel beam-to-column joints, only specimens with endplates of lower yield stresses can satisfy this design requirement.

6. Conclusions

The initial stiffness, plastic flexural moment capacities, ultimate moment capacities and ductility of the bolted high-strength steel beam-to-column joints are investigated through finite element analysis. The developed finite element models are validated against experimental results available in the literature and a series of parametric studies are performed. In addition, performance of the bolted high-strength steel beam-to-column joints with three different design details is compared. The benefits of using high-strength materials in beam-to-column joints are presented. Furthermore, the mechanical performance of the high-strength steel beam-to-column joints are compared with the current design codes. The results obtained from the finite element analysis were analysed and the following conclusions can be drawn:

- The developed finite element model includes the fracture of materials, through which the performance of bolted high-strength steel beam-to-column joints can be accurately predicted. It is also demonstrated that the self-weight of the bolted beam-to-column joints can be reduced by 40% through using high-performance materials;
- Comparisons between the connections of different design details are carried out. It is found that the high-strength steel beam-to-column joints with both extended endplates and flush endplates can be categorised into semi-rigid connections. However, the extended endplate connections perform better than the connections with flush endplates in terms of

the initial stiffness and plastic flexural moment capacities;

- According to the parametric analysis, it is found that the bolt strength, endplate thickness and strength are the critical parameters for the design of bolted steel beam-to-column joints. Generally, these design parameters have proportional effects on the initial stiffness and plastic flexural moment capacities. However, adverse influences on the ductility performance of the connections can also be observed.
- Comparisons between the numerical results and EC3-1-8 (2005) indicate that the elastic distribution design concept is over-conservative for high-strength steel beam-to-column joints. However, the current plastic analysis methods in EC3-1-8 (2005) for predicting the initial stiffness and plastic flexural moment capacities of the high-strength steel beam-to-column joints are slightly unsafe. Proper modifications are required to improve the reliability and safety of the design methods.
- Further experimental studies on the T-stub connections with high-strength materials are suggested to confirm the yield line patterns. If the yield line patterns are similar to the existing ones made from conventional mild steel. The authors would recommend the reduction factors to be further reduced when high-strength materials are utilised. This procedure will easily facilitate the plastic design of high-strength steel beam-to-column joints to be included into the current EC3-1-8 (2005).
- Rotational capacity and ductility of the high-strength steel beam-to-column joints are assessed with the current design methods, which are developed for the conventional mild steel structures. It is concluded that the rotational capacities of the high-strength steel connections can still satisfy the design criterion.

Acknowledgments

The research described in this paper is financially supported by the Australian Research Council (ARC). The first author is supported by the Australian Research Council (ARC) under its Discovery Scheme (Project No: DP170100001). The financial support is gratefully acknowledged.

References

ABAQUS 6.16, (2016), Computer software, Dassault systems, Waltham, MA, USA.

Abidelah, A., Bouchair, A. and Kerdal, D.E. (2012), "Experimental and analytical behaviour of bolted end-plate connections with or without stiffeners", *J. Constr. Steel Res.*, **76**, 13-27.

AS4100-1998 (1998), Standards Australia, Steel structures.

AS/NZS 5100.6-2017 (2017), Standards Australia, Bridge Design, Part 6: Steel and Composite Construction.

AS/NZS 2327-2017 (2017), Standards Australia, Composite structures-composite steel-concrete construction in buildings.

Augusto, H., Silva, L.S.D., Rebelo, C. and Castro, J.M. (2016), "Characterization of web panel components in double-extended bolted end-plate steel joints", *J. Constr. Steel Res.*, **116**, 271-293.

Ban, H.Y., Shi, G., Shi, Y. and Bradford, M.A. (2013), "Experimental investigation of the overall buckling behaviour of 960 MPa high strength steel columns", *J. Constr. Steel Res.*, **88**, 256-266.

Chen, J., Young, B. and Uy, B. (2006), "Behaviour of high strength structural steel at elevated temperatures", *J. Constr. Steel Res.*, **132**(12), 1948-1954.

Coelho, A.M.G. and Bijlaard, F.S.K. (2007), "Experimental behaviour of high strength steel end-plate connections", *J. Constr. Steel Res.*, **63**, 1228-1240.

Coelho, A.M.G., Simoes, D.S.L. and Bijlaard, F.S.K. (2006), "Ductility analysis of bolted extended endplate beam-to-column connections in the framework of the component method", *Steel Compos. Struct., Int. J.*, **6**(1), 33-53.

Du, Y., Chen, Z., Liew, J.Y.R. and Xiong, M.X. (2017), "Rectangular concrete-filled steel tubular beam-columns using high-strength steel: Experiments and design", Journal of constructional steel research, 131: 1-18.

Eurocode 3 (2005), Design of Steel Structures-Part 1-8: Design of joints, BS EN 1993-1-12, London, UK.

Eurocode 3 (2007), Design of Steel Structures-Part 1-12: Additional rules for the extension of EN1993 up to steel grades S700, BS EN 1993-1-12, London, UK.

Francavilla, A.B., Latour, M., Piluso, V. and Rizzano, G. (2018), "Design of full-strength full-ductility extended end-plate beam-to-column joints", *J. Constr. Steel Res.*, **148**, 77-96.

Ge, H., Jia, L.J., Kang, L. and Suzuki, T. (2014), "Experimental study on seismic performance of partial penetration welded steel beam-to-column joints with different fillet radii", *Steel Compos. Struct., Int. J.*, **17**(6), 851-865.

Gholami, M., Deylami, A. and Tehranizadeh, M. (2013), "Seismic performance of flange plate connections between steel beams and box columns", *J. Constr. Steel Res.*, **84**, 36-48.

Gogou, E. (2012), "Use of high strength steel grades for economical bridge design", Master Thesisl Delft University of Technology, Netherlands.

Goswami, R. and Murty, C.V.R. (2010), "Externally reinforced welded I-beam-to-box-column seismic connection", *J. Constr. Steel Res.*, **136**(1), 23-30.

Günther, H-P. (2005), "Use and Application of High-performance Steels for Steel Structures", International Association for Bridge and Structural Engineering (IABSE); Structural Engineering Documents, Vol. 8.

Johnson, G.R. and Cook, W.H. (1985), "Fracture characteristics of three metals subjected to various strains, strain rates, temperatures and pressures", *Eng. Fract. Mech.*, **21**(1), 31-48.

Kim, Y.J. and Oh, S.H. (2007), "Effects of moment transfer efficiency of a beam web on deformation capacity at box column-to-H beam connections", *J. Constr. Steel Res.*, **63**, 24-36.

Li, D., Uy, B., Patel, V. and Aslani, F. (2016a), "Behaviour and design of demountable steel column-column connections", *Steel Compos. Struct., Int. J.*, **22**(2), 429-448.

Li, D., Uy, B., Aslani, F. and Patel, V. (2016b), "Analysis and design of demountable steel column-baseplate connections", *Steel Compos. Struct., Int. J.*, **22**(4), 753-775.

Li, T.J., Li, G.Q., Chan, S.L. and Wang, Y.B. (2016c), "Behaviour of Q690 high-strength steel columns: Part 1: Experimental investigation", *J. Constr. Steel Res.*, **123**, 18-30.

Li, D., Uy, B., Aslani, F. and Patel, V. (2018), "Behaviour and design of demountable CFST column-column connections under tension", *J. Constr. Steel Res.*, **138**, 761-773.

Liu, X.C., Yang, Z.W., Wang, H.X., Zhang, A.L., Hu, S.H., Chai, S.T. and Wu, L. (2017), "Seismic performance of H-section beam to HSS column connection in prefabricated structures", *J. Constr. Steel Res.*, **138**, 1-16.

Mirghaderi, S.R., Torabian, S. and Keshavarzi, F. (2010), "I-beam to box-column connection by a vertical plate passing through the column", *Eng. Struct.*, **32**, 2034-2048.

Morrison, M., Quayyum, S. and Hassan, T. (2017), "Performance enhancement of eight bolt extended end-plate moment connections under simulated seismic loading", *Eng. Struct.*, **151**, 444-458.

Oh, S.H. and Park, H.Y. (2016), "A study to enhance the deformation capacity of beam-to-column connections using high strength steel having high yield ratio", *Int. J. Steel Struct.*, **16**(1), 73-89.

Portoles, J.M., Serra, E. and Romero, M.L. (2013), "Influence of ultra-high strength infill in slender concrete-filled steel tubular columns", *J. Constr. Steel Res.*, **86**, 107-114.

Qiang, X., Bijlaard, F.S.K., Kolstein, H. and Jiang, X. (2014), "Behaviour of beam-to-column high strength steel endplate connections under fire conditions-Part 1: Experimental study", *Eng. Struct.*, **64**, 23-38.

Qiang, X., Jiang, X., Bijlaard, F.S.K., Kolstein, H. and Luo, Y. (2015), "Post-fire behaviour of high strength steel endplate connections-Part 1: Experimental study", *J. Constr. Steel Res.*, **108**, 82-93.

Sabbagh, A.B., Chan, T.M. and Mottram, J.T. (2013), "Detailing of I-beam-to-CHS column joints with external diaphragm plates for seismic actions", *J. Constr. Steel Res.*, **88**, 21-33.

Shi, G., Shi, Y., Wang, Y. and Bradford, M.A. (2008), "Numerical simulation of steel pretensioned bolted end-plate connections of different types and details", *Eng. Struct.*, **30**, 2677-2686.

Shi, G., Ban, H. and Bijlaard, F.S.K. (2012), "Tests and numerical study of ultra-high strength steel columns with end restraints", *J. Constr. Steel Res.*, **70**, 236-247.

Skalomenos, K.A., Hayashi, K., Nishi, R., Inamasu, H. and Nakashima, M. (2016), "Experimental behaviour of concrete-filled steel tube columns using ultrahigh-strength steel", *J. Struct. Eng.*, **142**(9), 04016057.

Tahir, M.M., Mohammadhosseini, H., Ngian, S.P. and Effendi, M.K. (2018), "I-beam to square hollow column blind bolted moment connection: Experimental and numerical study", *J. Constr. Steel Res.*, **148**, 383-398.

Tartaglia, R., D'Aniello, M. and Landolfo, R. (2018), "The influence of rib stiffeners on the response of extended end-plate joints", *J. Constr. Steel Res.*, **148**, 669-690.

Thai, H.T., Uy, B., Khan, M., Tao, Z. and Mashiri, F. (2014), "Numerical modelling of concrete-filled steel box columns incorporating high strength materials", *J. Constr. Steel Res.*, **102**, 256-265.

Thai, H.T., Vo, T.P., Nguyen, T.K. and Pham, C.H. (2017), "Explicit simulation of bolted endplate composite beam-to-CFST column connections", *Thin-Wall. Struct.*, **119**, 749-759.

Uy, B. (2001), "Strength of short concrete-filled high strength steel box columns", *J. Constr. Steel Res.*, **57**(2), 113-134.

Uy, B., Patel, V., Li, D. and Aslani, F. (2017), "Behaviour and design of connections for demountable steel and composite structures", *Structures*, **9**, 1-12.

Vasdravellis, G. and Uy, B. (2014), "Shear strength and moment-shear interaction in steel-concrete composite beams", *J. Struct. Eng.*, **140**(11), 04014084.

Vasdravellis, G., Valente, M. and Castiglioni, C.A. (2009), "Behaviour of exterior partial-strength composite beam-to-column connections: Experimental study and numerical simulations", *J. Constr. Steel Res.*, **65**(1), 23-35.

Wang, J., Uy, B. and Li, D. (2018), "Analysis of demountable steel and composite frames with semi-rigid bolted joints", *Steel Compos. Struct., Int. J.*, **28**(3), 363-380.

Weynand, K. (1997), "Sicherheits-und Wirtschaftlichkeitsuntersuchungen zur Anwendung nachgiebiger Anschlüsse im Stahlbau", Heft, 35. Aachen: Shaker Verlag.

Wilkinson, S., Hurdman, G. and Crowther, A. (2006), "A moment resisting connections for earthquake resistant structures", *J. Constr. Steel Res.*, **62**, 295-302.

Xiong, M.X., Xiong, D.X. and Liew, J.Y.R. (2017), "Axial performance of short concrete filled steel tubes with high- and ultra-high-strength materials", *Eng. Struct.*, **136**, 494-510.

Xu, F., Chen, J. and Chan, T.M. (2017), "Numerical analysis and punching shear fracture based design of longitudinal plate to concrete-filled CHS connections", *Constr. Build. Mater.*, **156**(15), 91-106.

Zanon, P. and Zandonini, R. (1988), "Experimental analysis of endplate connections", *Proceedings of the State of the Art Workshop on Connections and the Behaviour of Strength and Design of Steel Structures*, Cachan, France, pp. 41-51.

DL